VNU Journal of Science: Mathematics - Physics

Journal homepage: https://js.vnu.edu.vn/MaP

Original Article

Free Vibration and Bending of Gradient Auxetic Plate Using Finite Element Method

Pham Hong Cong[1,*], Vu Dinh Trung[1], Do Duc Hai[2], Nguyen Dinh Khoa[2]

[1]*Centre for Informatics and Computing, Vietnam Academy of Science and Technology, 18 Hoang Quoc Viet, Hanoi, Vietnam*

[2]*VNU University of Engineering and Technology, 144 Xuan Thuy, Cau Giay, Hanoi, Vietnam*

Received 21 July 2021
Revised 02 August 2021; Accepted 02 August 2021

Abstract: In recent years, there has been a new approach to the material industry that uses sandwich structures with auxetic honeycomb cores with the interesting property of negative Poisson's ratios. In this paper, the Finite Element Method (in ANSYS) is used to investigate natural frequency of vibration and bending characteristics under varying pressure loads applied on the top skin when changing fundamental properties of some gradient configurations, including angular gradient, thickness gradient and functional gradient configurations of the auxetic plate with honeycomb structure. Thereby, the advantages of each configuration are investigated, studied, and obtained; therefore, it is expected to be applied in various industry sectors, such as wind turbine blades, aircraft wings, among others.

Keywords: auxetic plate, gradient auxetic, free vibration and bending, Finite Element Method

Nomenclature

t	The thickness of the wall of honeycombs	E	Elastic module of material
l	The length of the wall of honeycombs	ρ	Density of material
θ	The inclined angle of the cells	ν	Poisson's ratio of material
h	Height of the plate	h_c	Width of single cell
L	Length of the plate	G	Shear moduli of material
h_1	The thickness of top layer		
h_2	The thickness of middle layer		
h_3	The thickness of top layer		

* Corresponding author.
E-mail address: phcong@cic.vast.vn

https//doi.org/10.25073/2588-1124/vnumap.4664

1. Introduction

Auxetic materials have been applied in many fields of industry, sports, the military, aeronautics because of their special characteristics. If they are under applied tension in a direction, the dimension of perpendicular directions will be increased. This means that the Poisson's ratio of these materials (which is given by $\upsilon_{xy} = -\varepsilon_y / \varepsilon_x$, where ε_x is an applied tensile strain and ε_y is the resulting tensile strain in the transverse direction) is negative [1].

In recent years, there have been a lot of published researches related to the auxetic material model. One of the most prominent studies is Tian and Chun [2] about wave propagation in sandwich panel with auxetic core using semi-analytical finite element method. Lira et al., [3] also published the gradient cellular core based on auxetic configurations, which could be applied in the aero-engine fan blades using the FEM combined with experimental results.

The bending and failure of sandwich structures with auxetic gradient cellular cores were investigated by Y. Hou Th al. [4] using the FEM model and experimental results. In 2016, Zhang and Yang [5] published an article about numerical and experimental studies of a light-weight auxetic cellular vibration isolation base. Numerical and experimental analyses were conducted to reveal the effects of Poisson's ratio (known as cell angle) and relative density (known as cell thickness) of the reentrant honeycombs on the dynamic performance of the novel base.

A new approach to study nonlinear dynamic response and vibration of sandwich composite cylindrical panels with auxetic honeycomb core layer was proposed by Duc Th al. [6]. In that study, the authors used the analytical methods based on Reddy's first order shear deformation theory (FSDT) to determine the panel's dynamic response and natural frequency. Furthermore, there were a series of studies that applied the analytical methods of the authors Duc and Cong [7-9] to investigate the nonlinear dynamic response and vibration of sandwich composite plates, geometrically nonlinear dynamic response of eccentrically stiffened circular cylindrical shells, the dynamic response and vibration of composite double curved shallow shells. In 2019, Meena and Singamneni [10] proposed a new auxetic structure with significantly reduced stress concentration effects using the analytical method combined with experimental method. Zhang Th al. [11] used the finite element method and experiment to research the dynamic crushing of gradient auxetic honeycombs. In the same year, Cong Th al. [12] studied static bending analysis of auxetic plate by using FEM and a new third-order shear deformation plate theory. Meanwhile, some authors, such as Tomasz Strek Th al. [13] and Shammo Dutta Th al. [14] also used the FEM to study auxetic beams under bending and auxetic plate deformation under tensile loads.

As can be seen from the above, none of those studies revealed that changes in gradient configurations, such as angular gradient, thickness gradient, functional gradient in the natural frequency and bending could affect the characteristics of the auxetic plate. Therefore, this work modeled three gradient configurations of auxetic core: angular gradient, thickness gradient, functional gradient and simulated the models using the FEM in ANSYS. As a result, the natural frequency and deformation of plate are obtained and the characteristics of each configuration are also remarked.

2. The Research Model and Methodology

2.1. The Research Model

This work investigates three configurations of auxetic plate: Angular gradient auxetic, thickness gradient auxetic, functional gradient auxetic that are specifically described below. The common

structure of three configurations of auxetic plate includes three layers: top and bottom skin layers are made of isotropic material, the internal skin or core is auxetic structure with different kinds of shape and material (Figure 1).

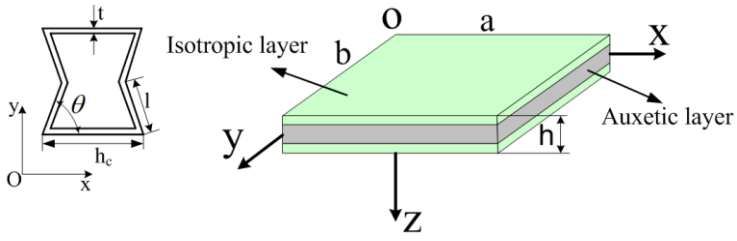

Figure 1. Geometric parameters of a cell in honeycomb core and auxetic plate.

Formulas in reference [2] are adopted to calculate honeycomb core material property:

$$E_1^C = E\left(\frac{t}{l}\right)^3 \frac{\cos\theta}{\left(\frac{h_c}{l}+\sin\theta\right)\sin^2\theta}, E_2^C = E\left(\frac{t}{l}\right)^3 \frac{\left(\frac{h_c}{l}+\sin\theta\right)}{\cos^3\theta} v_{12}^C = \frac{\cos^2\theta}{\left(\frac{h_c}{l}+\sin\theta\right)\sin\theta},$$

$$G_{12}^C = E\left(\frac{t}{l}\right)^3 \frac{\left(\frac{h_c}{l}+\sin\theta\right)}{\left(\frac{h_c}{l}\right)^2\left(1+2\frac{h_c}{l}\right)\cos\theta} G_{13}^C = G\frac{t}{l}\frac{\cos\theta}{\frac{h_c}{l}+\sin\theta}, G_{23}^C = G\frac{t}{l}\frac{1+2\sin^2\theta}{2\cos\theta\left(\frac{h_c}{l}+\sin\theta\right)}, \quad (1)$$

$$\rho^C = \rho\frac{t/l\left(h_c/l+2\right)}{2\cos\theta\left(h_c/l+\sin\theta\right)},$$

where symbol "c " represents core material, E, G and ρ are Young's module, shear module and mass density of the origin material, respectively.

2.1.1. Angular Gradient Configurations

An angular gradient (AGA) negative Poisson's ratio honeycomb structure can be obtained by changing the inclined angle of the cells θ_n as shown in Figure 2. The cell inclined angle increases as the layer number of honeycombs increases as follows:

$$\theta_n = 30^o + (n-1)\times 5^o, (\theta_n < 90^o), \quad (2)$$

where n is layer number of the honeycombs.

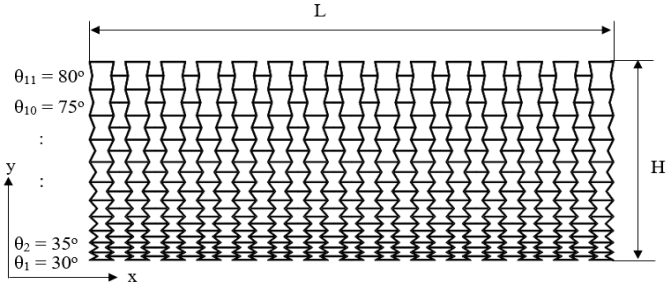

Figure 2. Angular gradient auxetic core.

2.1.2. Thickness Gradient Auxetic (TGA)

The second configuration gradient auxetic honeycombs can be obtained by changing the wall thickness of honeycomb cells t as shown in Figure 3. The cell walls thickness increases as the number of honeycombs layers increases with the growth of honeycomb layers as follows.

$$t_n = 0.0001 + 0.00002(n-1) \quad (3)$$

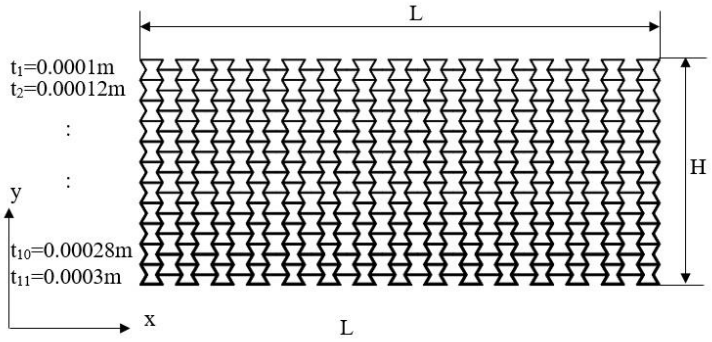

Figure 3. Thickness gradient auxetic core.

2.1.3. Functional Gradient Auxetic

Functional gradient auxetic (FGA) honeycombs as shown in Figure 4 are described as follows: the top of the honeycombs is metal, and the bottom is ceramic. The materials transit continuously along from metal to ceramic along y axis, the in-plane direction of the auxetic honeycombs. Moreover, the content of ceramic along the positive direction of y axis is gradually reduced. The content of ceramic is expressed by the following volume fraction [11]:

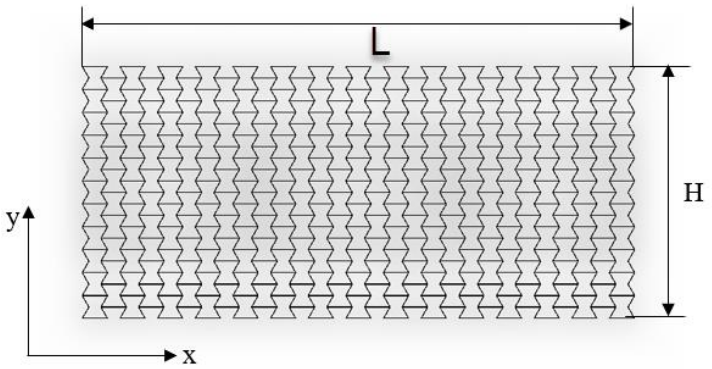

Figure 4. Functional gradient auxetic core.

2.2. Methodology

In this paper, the finite element method is applied to investigate the natural frequency of the auxetic plate model. Especially, ANSYS workbench with modal module would be used to simulate this problem.

The process flow chart of modal problem is shown in Figure 5.

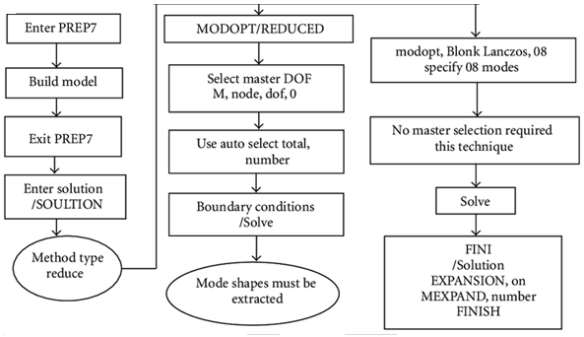

Figure 5. The process flow chart of modal problem [15].

For the Modal problem, it is expressed in matrix form as [16]:

$$[M]\{\ddot{u}\}+[C]\{\dot{u}\}+[K]\{u\}=\{F\}. \quad (4)$$

In this formula, the mass M, damping C and stiffness K matrices are constant with time and the unknown nodal displacements vary with time. The finite element method approximates the real structure with a finite number of degrees of freedom. In the model with N mode shapes, the real structure is found to have N degree of freedom with the finite element method.

In modal analysis of ANSYS software, the process to determine the N natural frequencies and mode shapes of the model, given initial conditions, such as boundary conditions and material properties for each part of the model. The structure model will vibrate at one of its natural frequencies and the shape of the vibration will be a scalar multiple of a mode shape, given "arbitrary" initial conditions. The resulting vibration will be a superposition of mode shapes, determines the vibration characteristics (natural frequencies and mode shapes) of a structural component. Natural frequencies and mode shapes are starting point for a transient or harmonic analysis if using the mode superposition method.

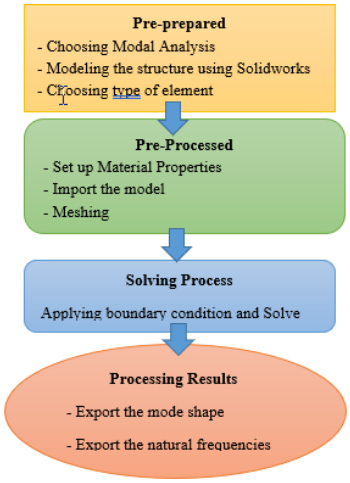

a) Natural frequency analysis diagram.

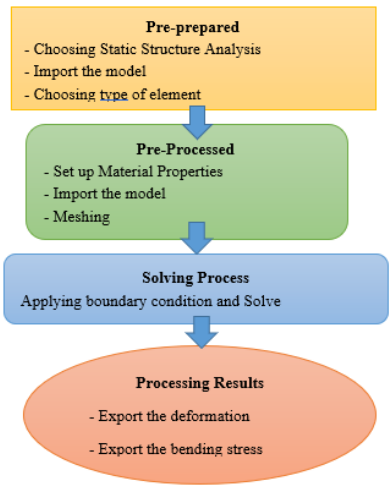

b) Static structural analysis diagram.

Figure 6. The flow chart to solve the natural frequency and bending problem in ANSYS software.

Basically, the chart has 4 steps to solve the natural frequency and bending problems: Pre-prepared, preprocessed, solving process, processing results. In each step, there are small tasks or sub-steps shown in Figure 6.

3. Results and Discussion

3.1. Verification Study

Example 3.1.1: In this part, a simple model of the isotropic plate is modelled and simulated in ANSYS software to examine the validity of the method in this research. A square plate with four clamped edges (side a =1) under uniform transverse pressure $(F=1)$, and the thickness h. The elastic module is taken as $E=10,9201$, and the Poisson's ratio is chosen as $\nu=0.3$.

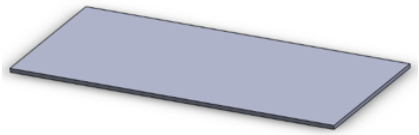

Figure 7. The isotropic material plate.

The non-dimensional transverse displacement is set as

$$\bar{w}=w\frac{D}{Pl^4}, \tag{5}$$

where the bending stiffness D is taken as

$$D=\frac{Eh^3}{12\left(1-\nu^2\right)} \tag{6}$$

Table 1. Comparison of $\bar{W}$ with the results of Ref. [12].

a/h	Mesh	Ref. [12]	Present
$a/h=10$	2x2	0.00357	0.0015424
	6x6	0.001486	0.0014009
	10x10	0.001498	0.0014325
	20x20	0.001503	0.0014916
	30x30	0.001503	0.0014989

Table 1 shows that there is almost total agreement between the results of the present paper and the results of the study in Ref [12]. This means that the method used in this research is valid.

Example 3.1.2: Considering a square plate with the edge length $a=1$ m, the thickness $h=0.02$ m. The material of the plate is steel with these parameters: density: $\rho=7850$ kg/m^3, the elastic Young's module $E=2\times10^{11}$ Pa, Poisson's ratio $\nu=0.3$. The square plate is clamped in 2 edges, which means:

$$\mathrm{w}_0^z=0,\mathrm{w}_a^z=0,\mathrm{w}_0^x=0,\mathrm{w}_a^x=0,\mathrm{w}_0^y=0,\mathrm{w}_a^y=0 \tag{7}$$

and

$$\frac{\partial \mathrm{w}_0^z}{\partial z}=0;\frac{\partial \mathrm{w}_a^z}{\partial z}=0;\frac{\partial \mathrm{w}_0^x}{\partial x}=0;\frac{\partial \mathrm{w}_a^x}{\partial x}=0;\frac{\partial \mathrm{w}_0^y}{\partial y}=0;\frac{\partial \mathrm{w}_a^y}{\partial y}=0; \tag{8}$$

Table 2. Comparison of results of critical natural frequency and maximum deformation of the plate.

Mode	Frequency (Hz)			Max deformation (mm)		
	Present	Ref. [12]	Error	Present	Ref. [12]	Error
1	107.65	107.9	0.24%	4.5136	4.5143	0.0066%
2	127.82	128.1	0.21%	6.8367	6.8385	0.003%
3	210.24	210.6	0.17%	7.4154	7.4719	0.053%
4	295.96	296.74	0.26%	4.5586	4.556	0.06%
5	324.26	325.11	0.259%	6.5444	6.5421	0.035%
6	384.31	384.8	0.127%	7.5434	7.548	0.06%
7	421.21	422.25	0.247%	6.8746	6.8763	0.0247%
8	578.16	579.94	0.307%	4.722	4.7202	0.038%
9	596.1	597.47	0.23%	7.2254	7.3154	0.124%
10	608.89	610.77	0.3%	6.5894	6.6952	0.16%
11	657.49	658.27	0.12%	7.3052	7.3154	0.134%
12	715.23	711.4	0.4%	6.6195	6.6124	0.1%

After analyzing the process in Ansys, there is a negligible difference of about 0.4% between the data of the obtained results and that of the analyzed results in the reference article [12].

Example 3.1.3: To solve this problem, the Auxetic sandwich panel with a length of $a = 154$ mm, another length of $b = 79.3$ mm and thickness $h = 0.22$ m; the thickness of the shell itself is $t_f = 12$ mm, horizontal ribs length $l = 12$ mm, vertical ribs length $h_d = 12$ mm, the angle between the horizontal ribs and the vertical ribs is $\theta = 80$ degrees, is considered.

A force (which is load cell) with magnitude $F = 5kN$ is applied on the plate's centre. Three rigid rollers having 12 mm of diameter act as loading and supporting devices. Rubber pressure pads of 12 mm width are placed between the bars and specimen to prevent inner damage to the facial shell (Figure 8). The distance $S = 54mm$ between two supporting devices is made by titanium with Young's module $E = 1.103 \times 10^{11}$ Pa, Poisson's ratio $\nu = 0.34$, and density $\rho = 4430$ kg/m^3 [4].

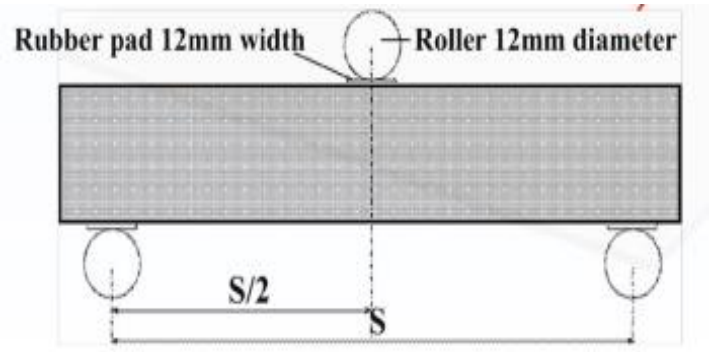

Figure 8. The configuration of the simulation model.

Table 3. Material configuration parameters of auxetic plate.

Parameters	Core (FDM ABSplus)	Shell (IM7/8552 carbon/epoxy unidirectional prepreg)
E_x (GPa)	2.02	171
E_y (GPa)	2.02	9.08
E_z (GPa)	1.53	9.08
G_{xy} (GPa)	0.705	5.29
G_{yz} (GPa)	0.705	3.97
G_{xz} (GPa)	0.626	5.29
ν_{xy}	0.43	0.32
ν_{yz}	0.43	0.5
ν_{xz}	0.43	0.32
ρ (kg/m^3)	1040	1430

With the variety of force: F_1 =0.5kN, F_2 =1.5kN, F_3 =2kN, F_4=4kN, F_5=6kN applied to the simulation model, the resulted deformations of the model are presented in Table 4, Figures 9 and 10.

Table 4. Comparison of the deformation results of gradient auxetic plate.

Force (N)	Ref. [4]	Present	Error
6kN	1.65	1.679	1.75%
5kN	1.38	1.3992	0.7%
4kN	1.12	1.1194	0.0536%
2kN	0.55	0.55968	1.7%
1.5k	0.42	0.419	0.23%
0.5k	0.14	0.13992	0.05%

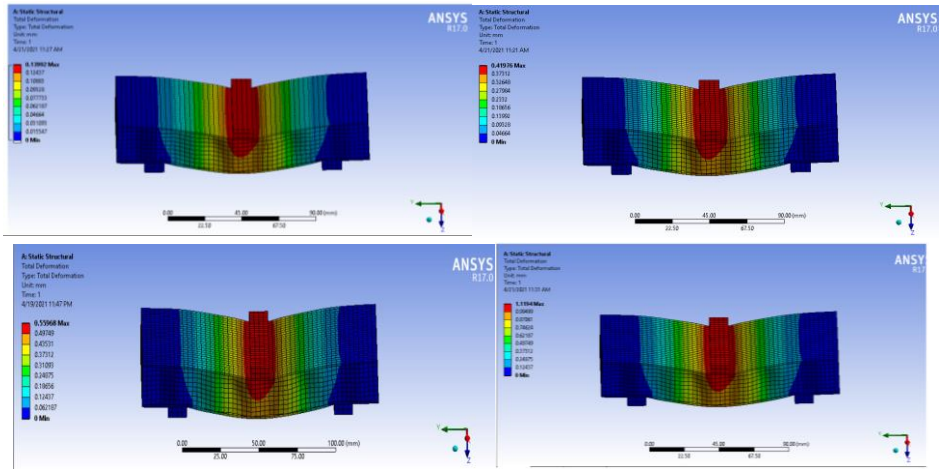

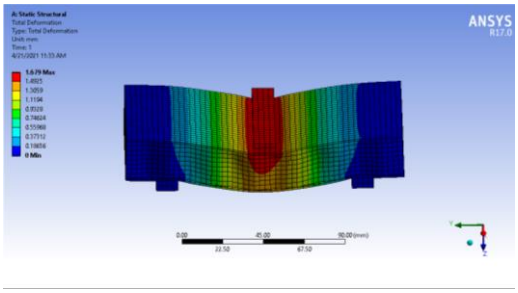

Figure 9. A variety of deformations with force: F_1 =0.5kN, F_2 =1.5kN, F_3 =2kN, F_4=4kN, F_5=6kN, respectively.

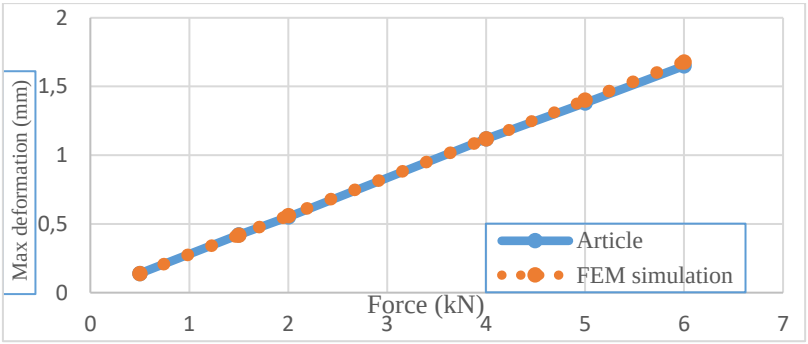

Figure 10. Comparing the maximum deformations (mm) of the gradient auxetic plate.

Table 4 and Figure 10 show an excellent agreement between the calculated results from the present paper and the results in the study of Ref. [4].

3.2. Simulation Results

3.2.1. Natural Frequency of Auxetic Plate

Example 3.2.1: This part presents the investigation of the thickness gradient auxetic plate made by the isotropic material: aluminium, with the thicknesses of the shell are: $h_1 = h_3 = 1$ mm, the auxetic core is manufactured with honeycomb shape using aluminium, the thickness of core layer is $h_2 = 3$ mm. The mechanical properties of aluminium: density $\rho = 2700\,\text{kg/m}^3$, the Elastic Young' module $E = 69\,\text{GPa}$, Poisson's ratio $\nu = 0.33$, the shear module $G = 26\,\text{GPa}$. The geometric parameters of single-core cell: $h = 4$ mm, $l = 2$ mm, $\theta = 60^\circ$, and the thicknesses of each layer's wall cells are shown in Table 5.

Table 5. Parameters of each layer of auxetic core.

Layer	Thickness t	Layer	Thickness t
1st layer	0.1 mm	7th layer	0.22 mm
2nd layer	0.12 mm	8th layer	0.24 mm
3rd layer	0.14 mm	9th layer	0.26 mm
4th layer	0.16 mm	10th layer	0.28 mm
5th layer	0.18 mm	11th layer	0.30 mm
6th layer	0.2 mm		

Appling the boundary condition CCCC to the 4 edges of the auxetic plate, the formulae of each edge are shown below:

$$\begin{aligned} &w_0^z = 0, w_L^z = 0, w_0^x = 0, w_L^x = 0, w_0^y = 0, w_L^y = 0 \\ &w_0^z = 0, w_H^z = 0, w_0^x = 0, w_H^x = 0, w_0^y = 0, w_H^y = 0 \end{aligned} \tag{7}$$

and

$$\begin{aligned} &\frac{\partial w_0^z}{\partial z} = 0; \frac{\partial w_L^z}{\partial z} = 0; \frac{\partial w_0^x}{\partial x} = 0; \frac{\partial w_L^x}{\partial x} = 0; \frac{\partial w_0^y}{\partial y} = 0; \frac{\partial w_L^y}{\partial y} = 0; \\ &\frac{\partial w_0^z}{\partial z} = 0; \frac{\partial w_H^z}{\partial z} = 0; \frac{\partial w_0^x}{\partial x} = 0; \frac{\partial w_H^x}{\partial x} = 0; \frac{\partial w_0^y}{\partial y} = 0; \frac{\partial w_H^y}{\partial y} = 0; \end{aligned} \tag{8}$$

After solving the formulae with simulation, we obtain:

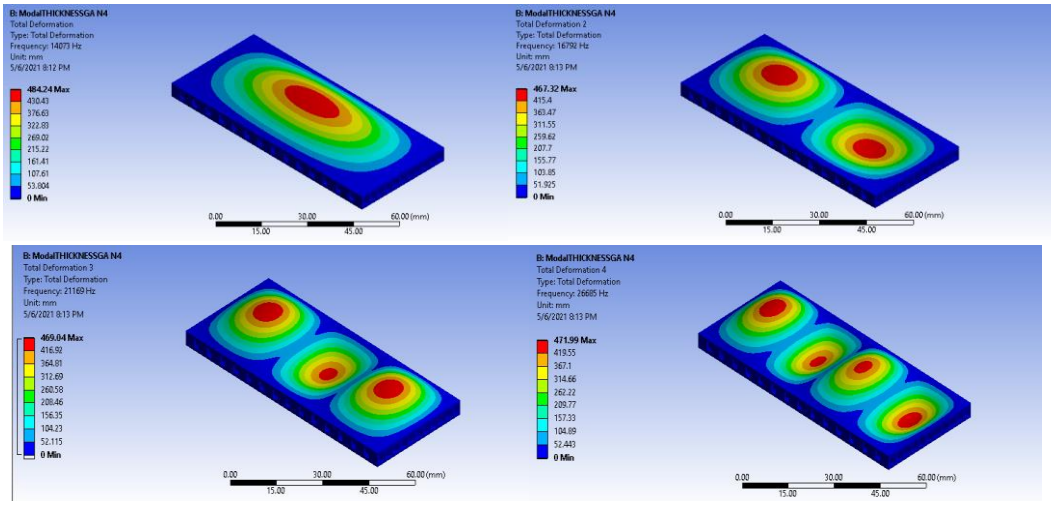

Figure 11. Shape Modes from 1 to 4 of thick auxetic plate.

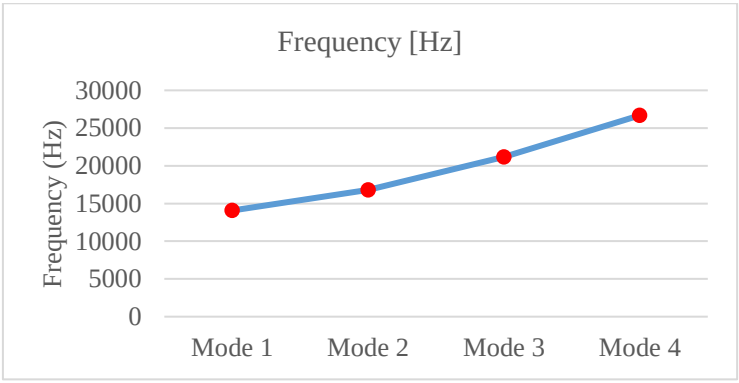

Figure 12. Chart for the varieties of frequency of thick auxetic plate.

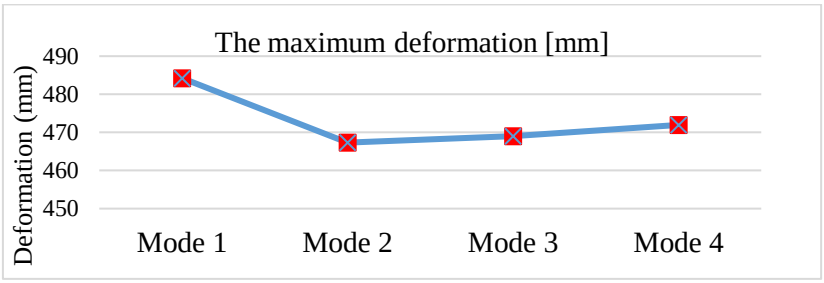

Figure 13. The maximum deformation across the thickness of auxetic plate.

Example 3.2.2: The angular gradient auxetic plate made of the isotropic material aluminium with the thicknesses of the plate: $h_1 = h_3 = 1$ mm is considered. The auxetic core is manufactured by honeycomb shape using aluminium with the thickness of core layer $h_2 = 3$ mm. The specifications parameters of aluminium: density $\rho = 2700$ kg/m3, the Elastic Young' module $E = 69$ GPa, Poisson's ratio $\nu = 0.33$, the shear module $G = 26$ GPa. The geometric parameters of single core cell are: $h = 4$ mm, $t = 0.15$ mm, the length of the wall cells of each layer and the angle concave of single cell are shown in Table 6.

Table 6. Parameters of each layer of angular gradient auxetic core.

Parameter	θ (º)	l (mm)
1st layer	30	1.4
2nd layer	35	1.5
3rd layer	40	1.6
4th layer	45	1.7
5th layer	50	1.8
6th layer	55	1.9
7th layer	60	2
8th layer	65	2.1
9th layer	70	2.2
10th layer	75	2.3
11th layer	80	2.4

After the simulation process with the same boundary conditions, the deformation, natural frequency, and the shape modes of the AGA plate are shown in Figures 14 - 16.

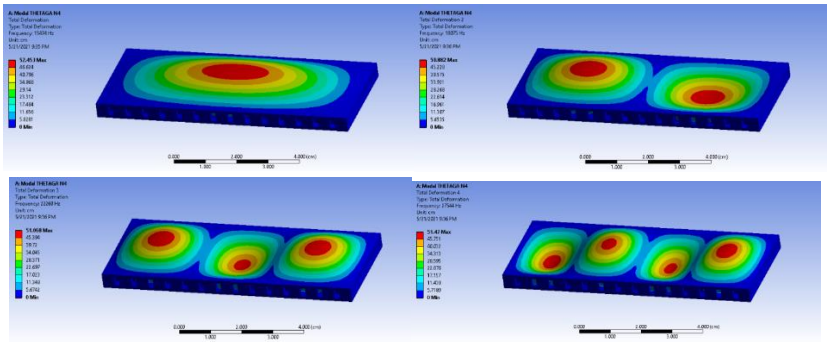

Figure 14. Shape Modes from 1 to 4 of angular auxetic plate.

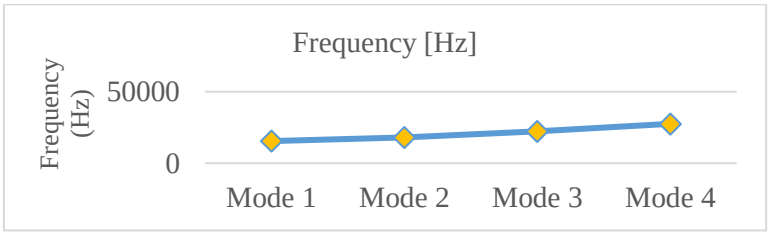

Figure 15. The frequency of Angular Auxetic plate.

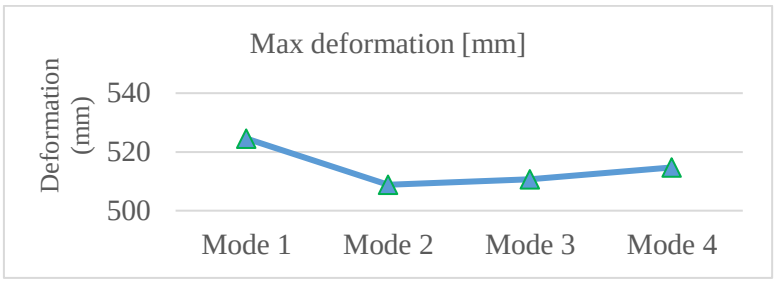

Figure 16. The maximum deformation of angular auxetic plate.

Example 3.2.3: The dimensions of the functional gradient auxetic model are almost the same as that of gradient auxetic one except the thickness of core wall. In this model, the thickness of the core wall is a constant value $t = 0.15$ mm. Each layer of this model has its own mechanical properties, which are shown in Table 7. After the simulation process with the same boundary conditions, the deformation, natural frequency, and the shape modes of the AGA plate are shown in Figures 17 - 19.

Table 7. Parameters of each layer of functional gradient auxetic core.

Parameter	Young's module [GPa]	Density [kg/m3]	Poisson's ratio
1st layer	69	2700	0.3
2nd layer	107.1	2750	0.294
3rd layer	145.2	2800	0.288
4th layer	183.3	2850	0.282
5th layer	221.4	2900	0.276
6th layer	259.5	2950	0.27
7th layer	297.6	3000	0.264
8th layer	335.7	3050	0.258
9th layer	373.8	3100	0.252
10th layer	411.9	3150	0.246
11th layer	450	3200	0.24

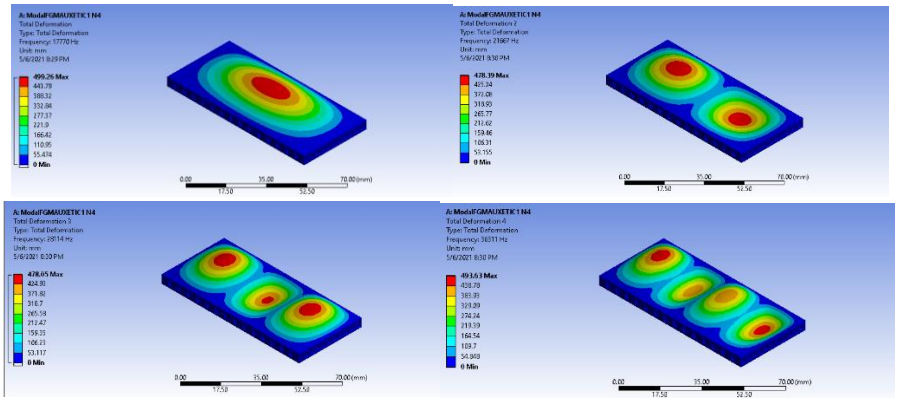

Figure 17. Shape modes from 1 to 4 of functional auxetic plate.

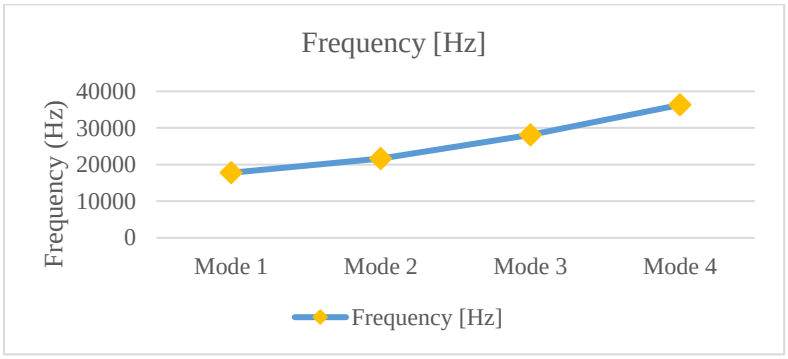

Figure 18. The frequency of functional auxetic plate.

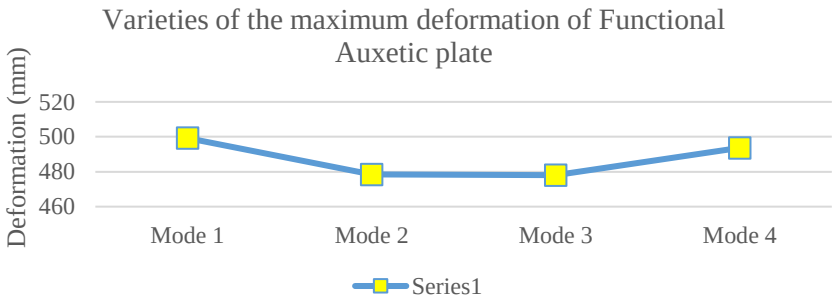

Figure 19. The maximum deformation of functional auxetic plate.

3.2.2. Bending of Auxetic Plate

Example 3.2.4: Using the same model as Section 3.2.1 with its mechanical properties remained unchanged, the applied boundary condition to the model is clamped for four edges of the plate. When the external force is applied, the outer surface of top shell is under pressure of magnitude 1000 Pa. After exporting the deformation of the plate, we obtain the results below:

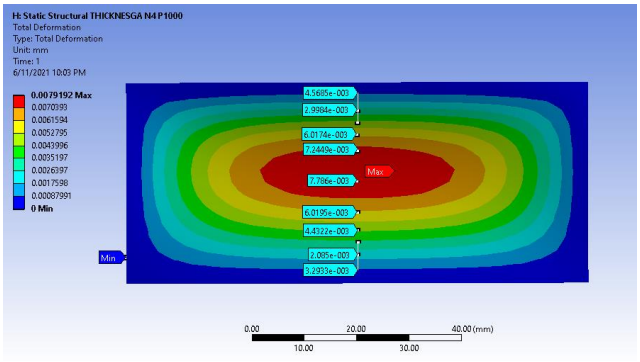

Figure 20. The deformation in centerline of auxetic plate.

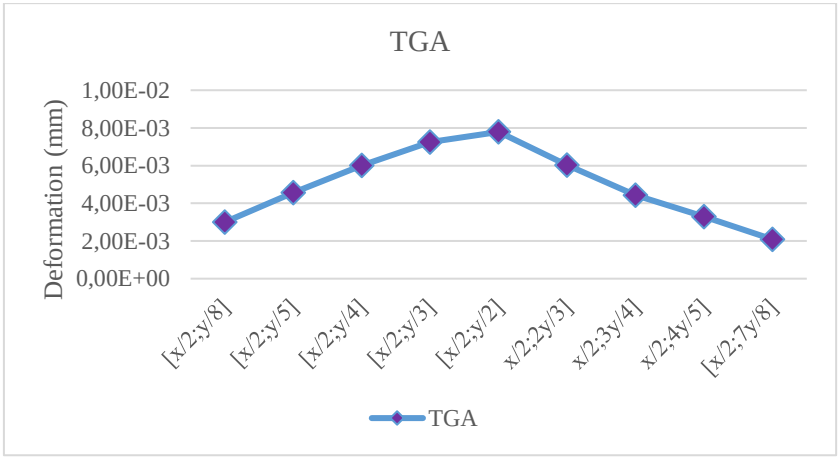

Figure 21. The deformation (mm) in the middle line of the TGA plate.

Example 3.2.5: With the same model of angular gradient auxetic as Section 3.2.1, a pressure with the magnitude of 1000 Pa is applied on the top surface of the auxetic plate. The obtained deformation results are shown in Figures 22 and 23:

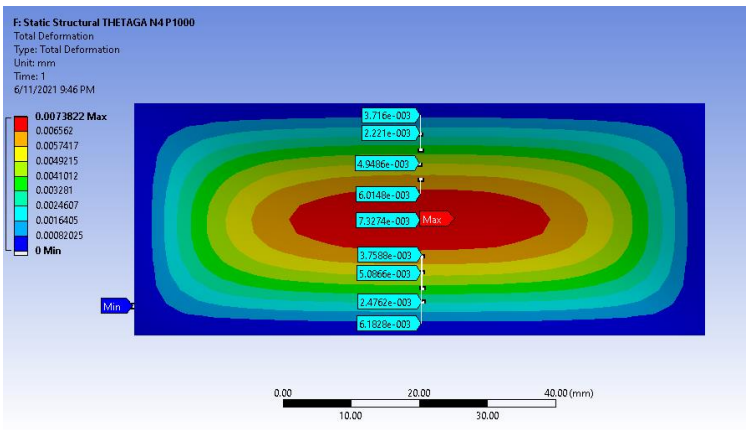

Figure 22. Deformation of AGA.

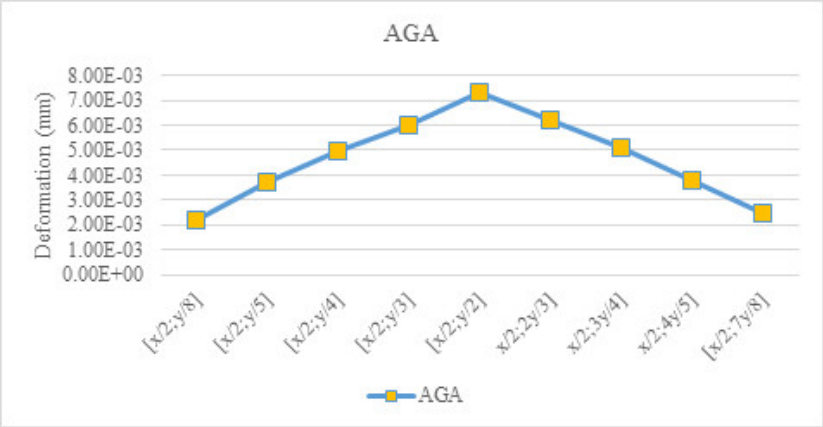

Figure 23. The deformation (mm) in the center line of the AGA plate.

Example 3.2.6: With the same model of angular gradient auxetic as Section 3.2.1, a pressure with the magnitude of 1000 Pa is applied on the top surface of the auxetic plate. The obtained deformation results are shown in the figures below:

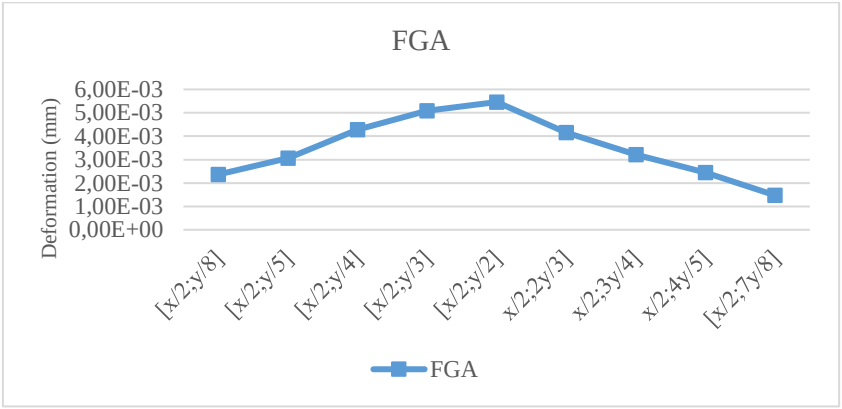

Figure 24. The deformation (mm) in the center line of the FGA plate.

Table 8. Varieties of the applied pressure magnitude of gradient auxetic and maximum deformation (mm),

Gradient Auxetic Configurations	AGA	TGA	FGA
500N	0.0036911	0.0039596	0.0028182
1000N	0.0073822	0.0079192	0.0056364
1500N	0.011073	0.011879	0.0084547
2000N	0.014764	0.015838	0.011273
2500N	0.018456	0.019798	0.014091

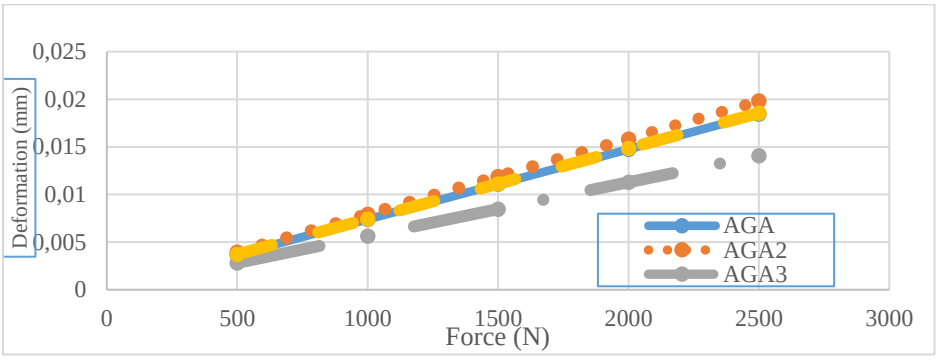

Figure 25. Deformation of gradient auxetic plates under different pressure values. Comparing the deformation of points in the middle line of the plate with $x = a/2$ and $y = 0 \to b$.

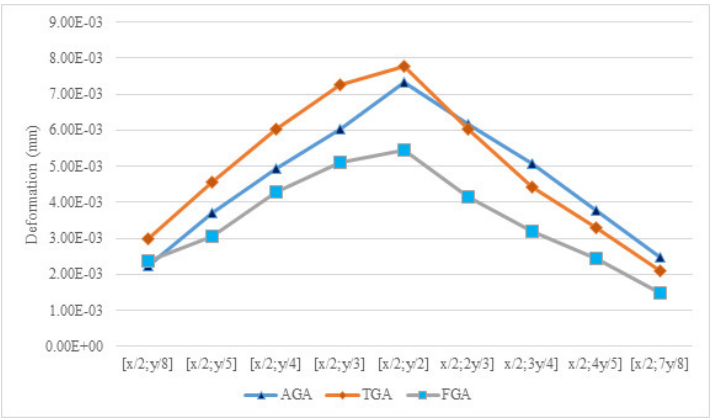

Figure 26. Curves of the deformation of points along the middle line of three types of auxetic gradient plate.

From the figures above, the deformation lines separated by the middle line went into two different directions. This is due to the changing of different material properties, such as the angle of core, the thickness, and elastic Young's module. In practical applications, this characteristic can be utilized for manufacturing purposes, such as producing the blade of an electric turbine, aeroplane wing, etc. needed to be resistant under changing working conditions.

4. Conclusion

This paper investigates the natural frequency and bending of the plate under various auxetic configurations with negative Poisson's ratio. By applying the finite element method with estimated simulation then comparing the results to published articles, this work is proven valid. The natural frequencies of four-shape mode and its maximum deformation of three types of configurations of the auxetic plate are explicitly indicated. The acquired results have practical meaning for industrial manufacturing since they can be applied in producing aircraft wings and other productions. In addition, this work solves the bending problem of three types of gradient configurations of the auxetic plate under various pressure values. The variability of deformation characteristics along the gradient direction could lead to many potential applications in the material industry in the future.

Acknowledgments

This research was funded by Vietnam Academy of Science and Technology under Grant VAST01.02/21-22.

References

[1] K. E. Evans, M. Nkansah, I. J. Hutchison, S. C. Rogers, Molecular Network Design, Nature, Vol. 353, No. 124, 1991, pp. 124-125, https://doi.org/10.1038/353124a0.

[2] D. Q. Tian, Y. Z. Chun, Wave Propagation in Sandwich Panel with Auxetic Core, Journal of Solid Mechanics, Vol. 2, No. 4, 2010, pp. 393-402.

[3] C. Lira, F. Scarpa, R. Rajasekaran, A Gradient Cellular Core for Aeroengine Fan Blades Based on Auxetic Configurations, Journal of Intelligent Material Systems and Structures, Vol. 22, 2011, https://doi.org/10.1177/1045389X11414226.

[4] Y. Hou, Y. H. Tai, C. Lira, F. Scarpa, J. R. Yates, B. Gu, The Bending and Failure of Sandwich Structures with Auxetic Gradient Cellular Cores, Composites: Part A, Vol. 49, 2013, pp. 119-131, https://doi.org/10.1016/j.compositesa.2013.02.007.

[5] X. W. Zhang, D. Q. Yang, Numerical and Experimental Studies of a Light - Weight Auxetic Cellular Vibration Isolation Base, 2016, pp. 1-16, https://doi.org/10.1155/2016/4017534.

[6] N. D. Duc, S. E. Kim, N. D. Tuan, T. Phuong, N. D. Khoa, New Approach to Study Nonlinear Dynamic Response and Vibration of Sandwich Composite Cylindrical Panels with Auxetic Honeycomb Core Layer, Aerospace Science and Technology, Vol. 70, 2017, pp. 396-404, https://doi.org/10.1016/j.ast.2017.08.023.

[7] N. D. Duc, P. H. Cong, Nonlinear Dynamic Response and Vibration of Sandwich Composite Plates with Negative Poisson's Ratio in Auxetic Honeycombs, Journal of Sandwich Structures and Materials, Vol. 20, No. 6, 2018, pp. 692-717, https://doi.org/10.1177/1099636216674729.

[8] P. H. Cong, P. T. Long, N. V. Nhat, N. D. Duc, Geometrically Nonlinear Dynamic Response of Eccentrically Stiffened Circular Cylindrical Shells with Negative Poisson's Ratio in Auxetic Honeycombs Core Layer, International Journal of Mechanical Sciences, Vol. 152, 2019, pp. 443-453, https://doi.org/10.1016/j.ijmecsci.2018.12.052.

[9] N. D. Duc, K. S. Eock, P. H. Cong, N. T. Anh, N. D. Khoa, Dynamic Response and Vibration of Composite Double Curved Shallow Shells with Negative Poisson's Ratio in Auxetic Honeycombs Core Layer on Elastic Foundations Subjected to Blast and Damping Loads, International Journal of Mechanical of Sciences, Vol. 133, 2017, pp. 504-512, https://doi.org/10.1016/j.ijmecsci.2017.09.009.

[10] K. Meena, S. Singamneni, A New Auxetic Structure with Significantly Reduced Stress Concentration Effects, Materials and Design, Vol. 173, 2019, pp. 107779, https://doi.org/10.1016/j.matdes.2019.107779.

[11] J. Zhang, B. Dong, W. Zhang, Dynamic Crushing of Gradient Auxetic Honeycombs, Journal of Vibration Engineering & Technologies, Vol. 11, 2020, https://doi.org/10.1007/s42417-020-00236-z.

[12] P. H. Cong, P. M. Phuc, H. T. Thiem, D. T. Manh, N. D. Duc, Static Bending Analysis of Auxetic Plate by FEM and a New Third-order Shear Deformation Plate Theory, VNU Journal of Science: Natural Sciences and Technology, Vol. 36, No. 1, 2020, pp. 90-99, https://doi.org/10.25073/2588-1140/vnunst.5000.

[13] T. Strek, B. Maruszewski, J. W. Narojczyk, K. W. Wojciechowski, Finite Element Analysis of Auxetic Plate Deformation, Journal of Non-Crystalline Solids, Vol. 354, 2008, pp. 4475-4480, https://doi.org/10.1016/j.jnoncrysol.2008.06.087.

[14] S. Dutta, H. G. Menon, M. P. Hariprasad, A. Krishnan, B. Shankar, Study of Auxetic Beams under Bending: A Finite Element Approach, Materials Today: Proceedings, 2020, https://doi.org/10.1016/j.matpr.2020.10.479.

[15] M. Abid, S. Maqsood, H. A. Wajid, Comparative Modal Analysis of Gasketed and Nongasketed Bolted Flamged Pipe Joints: FEA Approach, Advances in Mechanical Engineering, 2012, https://doi.org/10.1155/2012/413583.

[16] D. W. Herrin, Slides to Accompany Lectures in Vibro-Acoustic Design in Mechanical Systems 2012, KY 40506-0503.